https://doi.org/10.20965/jdr.2022.p0237

Note:

Numerical Simulation Study of Debris Particles Movement Characteristics by Smoothed Particle Hydrodynamics

Shoji Ueta*,†, Natsuki Hosono, Ryusuke Kuroki***, and Yosuke Yamashiki***

*Graduate School of Advanced Integrated Studies in Human Survivability, Kyoto University
1 Nakaadachi-cho, Yoshida, Sakyo-ku, Kyoto, Kyoto 606-8306, Japan
†Corresponding author, E-mail: showg1005@gmail.com
**Center for Mathematical Science and Advanced Technology, Japan Agency for Marine-Earth Science and Technology (JAMSTEC), Kanagawa, Japan
***Mizuho Bank, Ltd., Kyoto, Japan
[Received July 19, 2019; accepted December 28, 2021]

Debris flow is an important natural hazard in mountain zone because it can threaten human lives with very little warning. Since laboratory experiments on debris flows at real scale are difficult to perform, numerical simulations are important in evaluating the impact of such flows. Among several candidate models, the smoothed particle hydrodynamics (SPH) is a particular attractive numerical method for this purpose. SPH is a particle-based numerical hydrodynamic method originally developed in the astrophysical field before extension to elastic bodies. Several works have already tested the applicability of SPH to debris flow, despite there are only few detailed validations. In this report, thus, we aimed to check the applicability of SPH to debris flows. Since the accurate treatment of the elastic bodies tends to be computationally expensive, we have developed a massively parallel SPH code. A comparison between laboratory experiments and numerical simulations using SPH showed qualitatively similar features, though there are differences in quantitive comparisons.

Keywords: debris flow, numerical simulations, SPH

1. Introduction

Debris flow is an important natural hazard in mountain zone because its destructive features can threaten human lives. Laboratory experiments of full-scale debris flows are difficult; therefore, numerical simulations are important in evaluating their impact. Until now, many researches about debris flow have been performed, but the problems still remain to be solved (e.g., see [1]). Fundamental problem in applying numerical simulation is its computational scheme. Establishment of governing equations of debris flow based on solid-liquid mixed phase flow enables us in applying two-dimensional horizontal special scheme by depth-integrated governing equation as shallow-water-type flood analyses. This approach become very successful in practical application into real hazards, however the following uncertainty remains: (1) There are no practical three-dimensional approach of debris flow due to complexity in expressing free-surface boundary. Although it is technically possible to do it, huge difference in aspect ratio between horizontal and vertical grid spacing makes it almost impossible in practical application. (2) By applying depth integrated governing equations of debris flow deteriorate all complex discussions in developing their governing equations. To circumvent these issues, it is essential to numerically solve vertical motion of debris flow.

Euler-Lagrangian approach was performed in order to trace particle velocity in debris flow using Hydro-debris2D [2]. In their study velocity field of water flow was calculated using the Marker and Cell Method, which involves a Subgrid-Scale (SGS) model and the Particle Source in Cell (PSI-Cell) Method. The study performed good agreement of velocity distribution between numerical and laboratory experiments. At the same time, two dimensional constrain of the model disable them in applying more-realistic debris flow motion. Moreover, interaction between water (expressed using Eulerian equation) and sediment particles (expressed using Lagrangian equation) needs lots of empirical coefficients, such as virtual mass.

Recently, a particle-based numerical hydrodynamic scheme, smoothed particle hydrodynamics (SPH; [3, 4]), has been applied to numerical simulations of debris flow (e.g., [5, 6]). It was originally developed in the astrophysical field and was recently applied to numerical simulations of the natural hazards. Because SPH is Lagrangian in nature, it offers advantages to systems involving large deformations and multi-material flows. Debris flows have these features; therefore, SPH is an attractive approach for numerical simulations thereof.

In numerical simulations of debris flows, the interactions between solid and liquid can be important. Recently, Canelas et al. [5, 7] coupled the discrete element method (DEM) with SPH. They showed that the DEM-SPH successfully reproduced the experimental results of debris flows.

This approach, however, is limited in treating solid materials as rigid bodies. Thus, the deformation of materials is neglected. During large-scale debris flows, deformation

and breakdown of solid materials occur. These effects are important in predicting the actual damage to human lives.

One possible approach to overcome this problem is the incorporation of continuum mechanics with SPH. The elastic (and plastic) behaviors of solid materials in SPH have already been developed for impacts between celestial bodies [8]. In addition, recently, SPH was applied to simulations of the impacts of droplets on elastic planes (e.g., [9]). During the impact phenomenon, solid materials undergo high bulk compression and shear deformation. Debris flows are not as destructive as impact phenomena; however, this approach could be a useful way to perform numerical simulations of debris flows. However, no detailed comparisons exist for adopting this approach for debris flows.

One potential problem with this approach is that is computationally expensive. Unlike the DEM-SPH method, the approach must solve continuum bodies more accurately. In numerical simulations of fluids, the time step per step is determined by the size of the cell or particle and the speed of sound in the materials. The sound speeds of rocky materials tend to be much higher than that of water. Thus, it would be difficult to perform large-scale simulations.

In order to accelerate the speed of numerical simulations, we deployed the Framework for Developing Particle Simulator (FDPS, [10, 11]) software. FDPS is a general-purpose software suit used to perform massively parallel numerical simulations of arbitrary particle-based methods. Another way to accelerate the calculation speed is to reduce the sound speed. Monaghan [12] noted that, as long as the speed of sound is much higher than the "typical" speed of the fluid, the essential results are unchanged. However, it is unclear that whether this approach is applicable to multi-material flows.

There are several research works on debris flow focusing on a depth-integrated shallow-water equation based model for simulating debris flow fan and characteristics of grain concentration, etc. (e.g., [13, 14]). We also have used such a model for simulating mixture grain focusing on distribution of diameters and velocity in debris flow. In this survey, we focus first on the application of the Lagrangian approach using Smoothed Particles Hydrodynamics to simulate non-steady liquid and solid phase motion. Since this approach has not been studied yet, we focus for the first time on comparing the velocity distribution of grains and water motion all together. We also attempted to simulate a vertical two-dimensional numerical approach to simulate each grain with a velocity distribution simulation for all. However, such approach was not popular yet. Our proposed two-dimensional non-steady full Lagrangian SPH approach is new, and none of the past studies actually focus on a practical comparison with laboratory experiments for detailed flow motion. Full Lagrangian approach consisted by two-distinct particle (sediment and water phase) enables simpler and fundamental expression for most of the term associated with generating governing equation for mixture flow, and still generate vertical two-dimensional and full-three dimensional approach by avoiding free-surface boundary issue in Eulerian numerical simulation.

Also, in this study, in order to determine the applicability of reduced sound speeds to debris flows, we performed numerical simulations of debris flows by combining the above approaches. As a benchmark, we compared the results of the 2D numerical simulations with laboratory experiments like [15], but we use one-size particles. The experimental setup is similar to that in [15]; 20 kg of debris particles are placed on a slope and then flushed by water. In the experiments, after the water hit the debris particles, several debris particles pushed by the water preceded the water. Then, the water eroded the debris particles and carried them downstream. The detailed behaviors of the water and debris particles are recorded by a high-speed video camera (HSVC), thus, we can compare the behavior with the results of numerical simulations. Comparisons between laboratory experiments and numerical simulation using fully SPH manner are performed for the first time.

This report is organized as follows. In Section 2, we provide brief descriptions of SPH. In Section 3, we describe the numerical and experimental setup. In Section 4, we show the results of SPH and comparisons with the experimental results. In Section 5, we summarize the study.

2. Numerical Method

2.1. Basic Equations

The governing equations to describe the motions of fluids and solid bodies are as follows:

$$\frac{\mathrm{d}\rho}{\mathrm{d}t} = -\rho\nabla\cdot\vec{v}, \quad \ldots\ldots\ldots\ldots \quad (1)$$

$$\frac{\mathrm{d}\vec{v}}{\mathrm{d}t} = \frac{1}{\rho}\nabla\sigma + \vec{g}, \quad \ldots\ldots\ldots\ldots \quad (2)$$

where t, ρ, $\vec{v}$, σ, and $\vec{g}$ are the time, density, velocity, stress tensors, and the gravity acceleration, set to 9.8 m/s^2. Note that, in general cases, we must solve the equation of the energy. However, this is negligible for debris flows. Thus, we do not solve for the internal energy.

The stress tensor σ is important in expressing different materials. In the case of solid materials, σ can be expressed as

$$\sigma = -p\mathsf{E} + \mathsf{S}, \quad \ldots\ldots\ldots\ldots \quad (3)$$

where p is the pressure, E is the identified matrix, and S is the deviatoric stress tensor arising from the material strength. The first term describes the reactance of the material on the bulk compression (see below) and the latter term describes that of the shear deformation. The deviatoric stress tensor S is derived by directly integrating the derivative of it:

$$\frac{\mathrm{d}\mathsf{S}}{\mathrm{d}t} = 2\mu_0\left\{\frac{1}{2}\left[\nabla\otimes\vec{v} + (\nabla\otimes\vec{v})^{\mathrm{T}}\right] - \frac{1}{3}(\nabla\cdot\vec{v})\mathsf{E}\right\} + \mathsf{SR} - \mathsf{RS}, \quad \ldots\ldots\ldots\ldots \quad (4)$$

Table 1. Lists of material parameters used in this paper.

Name	c_0 [m/s]	ρ_0 [kg/m^3]	μ_0 [GPa]
Water	1400	1000	N/A
Basalt	3116	2750	22.7
Aluminum	5277	2700	25.5

where R is the rotation rate tensor given by:

$$\mathsf{R} = \frac{1}{2}\left[\nabla \otimes \vec{v} - (\nabla \otimes \vec{v})^{\mathrm{T}}\right]. \quad \ldots \quad (5)$$

The material parameter μ_0 is the shear modulus, which describes the strength of the materials under shear stress. The value depends on the kind of materials. In the case of Basalt, it is 22.7 GPa. In the case of Aluminum, it is 25.5 GPa (see Section 2.2).

On the other hand, for liquid materials, σ can be expressed as

$$\sigma = -p\mathsf{E} + \tau, \quad \ldots \quad (6)$$

where τ is the deviatoric stress tensor from the viscosity, given by:

$$\tau = 2\rho\nu_0 \times \left\{\frac{1}{2}\left[\nabla \otimes \vec{v} + (\nabla \otimes \vec{v})^{\mathrm{T}}\right] - \frac{1}{3}(\nabla \cdot \vec{v})\mathsf{E}\right\}, \quad (7)$$

where ν_0 is the kinetic viscosity, set to 10^{-6} m^2/s for water.

2.2. Equation of State

The pressure p is given by the function of the density (and, in the general case, the energy), referred to as the equation of states (EoS). Monaghan [12] applied the so-called Murnaghan EoS for weakly compressible flows in SPH. In this study, we applied a modified version of the Murnaghan EoS, vis., Birch-Murnaghan EoS. The simplest form of the Birch-Murnaghan EoS is

$$p = \frac{3}{2}\rho_0 c_0^2\left[\left(\frac{\rho}{\rho_0}\right)^{\frac{7}{3}} - \left(\frac{\rho}{\rho_0}\right)^{\frac{5}{3}}\right], \quad \ldots \quad (8)$$

where c_0 is the sound speed and ρ_0 is the density, which depends on the material. The subscription "0" denotes the value of the variable at the reference state.

Table 1 shows the values of these variables for each material used in this study, as given by [16]. Note that these values are not applied to the actual runs in this study; a numerical trick should be used for these values (for detail, see Section 2.4).

2.3. Equations of SPH

In SPH, fluids are represented as collections of hypothetical particles (SPH particles). The governing equations are converted into interactions between two particles. In SPH with multi-material system, each particle is assigned to one single material. In the following case, what we need to solve are the motions of water and debris. If a particle is assigned to water, we set σ to Eq. (6) and otherwise to Eq. (3). Note that there is no need to numerically solve the material mixture, because the motions of each particle reflect material mixtures. The motions of particles would result in important behaviors, such as entrainment and deposition. This is an advantage of SPH to other mesh methods. Since many reviews of SPH exist (e.g., [17]), here we provide only a brief summary of SPH.

There are two ways to obtain the density of each particle. In the first, the mass is summed for the particles surrounding particle i; in the second, the equation of continuity is evolved for each particle. Monaghan [12] reported that the latter approach was much more applicable to systems involving free surfaces. The widely accepted SPH expressions of divergence, rotation, and dyadic production are

$$\nabla * \vec{v}_i = \frac{1}{\rho_i}\sum_j m_j(\vec{v}_j - \vec{v}_i) * \nabla W(\vec{x}_j - \vec{x}_i; h_i), \quad . \quad (9)$$

where m is the mass of SPH particles, W is the so-called kernel function, the values noted in brackets of the kernel function are parameters, h is the smoothing length, $\vec{x}$ is the position vector, and $*$ is a placeholder operator in $* \in \{\cdot, \times, \otimes\}$.

The kernel function must be a compact support function. Amongst several forms of kernel functions, we employed the Wendland C6 kernel [18, 19] with the "kernel support width" $H = 2.5$. The value of smoothing length is determined by

$$h_i = \eta\left(\frac{m_i}{\rho_i}\right)^{\frac{1}{D}}, \quad \ldots \quad (10)$$

where D is the number of spatial dimensions and η is a factor which is typically set to 1.2. Note that kernel functions must be zero outside of Hh. Thus, Hh indicates the "interacting" radius and particle i regards other particles within Hh as particles composing a single continuum.

Then, the equation of continuity can be written as:

$$\frac{\Delta\rho_i}{\Delta t} = -\sum_j m_j(\vec{v}_j - \vec{v}_i) \cdot \nabla W(\vec{x}_j - \vec{x}_i; h_i), \quad . \quad (11)$$

the mass of the total system is conserved. Similarly, the equation of the motion can be written as:

$$\vec{a}_i = \sum_j m_j\left(\frac{\sigma_i}{\rho_i^2} + \frac{\sigma_j}{\rho_j^2} + \Pi_{ij}\right) \times \frac{1}{2}\left[\nabla W(\vec{x}_j - \vec{x}_i; h_i) + \nabla W(\vec{x}_j - \vec{x}_i; h_j)\right] + \vec{g}, \quad \ldots \quad (12)$$

where $\vec{a}$ is the acceleration, σ is the stress tensors, and $\vec{g}$ is the gravity acceleration, set to 9.8 m/s^2. SPH is a Lagrangian method, therefore, we set a kind of particles first, for example, basalt, water, and aluminum particles. Even if some materials interfuse, Eqs. (11) and (12) are true (e.g., [20]).

Here, Π is the so-called pair-wise artificial viscosity, which is necessary to address shocks. Amongst several forms of Π, we used that proposed in [21];

$$\Pi_{ij} = \begin{cases} -\frac{\alpha^{\rm AV}}{2}\frac{v_{ij}^{\rm sig} w_{ij}}{\rho_{ij}} & (w_{ij} < 0), \\ 0 \quad \text{(otherwise)}, \end{cases} \quad \ldots \quad (13)$$

$$w_{ij} = \frac{(\vec{x}_j - \vec{x}_i)\cdot(\vec{v}_j - \vec{v}_i)}{|\vec{x}_j - \vec{x}_i|}, \quad \ldots \quad (14)$$

$$v_{ij}^{\rm sig} = c_i + c_j - 3w_{ij}, \quad \ldots \quad (15)$$

$$\rho_{ij} = \frac{\rho_i + \rho_j}{2}, \quad \ldots \quad (16)$$

where c is the sound speed, given by:

$$c = \sqrt{\frac{{\rm d}p}{{\rm d}\rho}}. \quad \ldots \quad (17)$$

The parameter $\alpha^{\rm AV}$ determines the strength of the artificial viscosity (AV). Throughout this study, we set $\alpha^{\rm AV} = 1.0$. Note that this AV sometimes leads to a nonphysical shear force. Thus, we introduce the Balsara switch [22].

The size of time step for each step is controlled by the AV and the acceleration:

$$\Delta t_i = \min\left(C_{\rm CFL}\frac{2h_i}{\max_j v_{ij}^{\rm sig}}, C_{\rm f}\sqrt{\frac{h_i}{|\vec{a}_i|}}\right). \quad \ldots \quad (18)$$

Both $C_{\rm CFL}$ and $C_{\rm f}$ are set to 0.1 throughout this study. The time-stepping is done by a leap-frog integrator.

Here we note that the most important thing which distinguish given materials is σ given in Eqs. (3) and (6). Other variables and/or functions, such as the kernel function and $\nabla * \vec{v}$ do not have essential role to distinguish different materials. Hence, SPH does not require ad-hoc terms of the interactions between solid and liquid. Eq. (12) naturally introduces forces which acts on between solid and liquid.

2.4. Reduction of the Sound Speed and Time Step Criteria

Recall that the EoS employed in this study is given in Eq. (8). However, we note that the typical sound speeds of the materials used in this study are much higher than that in bulk flows of water. It has been reported that for sound speeds much higher than that of the bulk speed of flows, the results are not changed significantly [12]. [12] performed a dam break problem by reducing sound speed of water (1400 m/s) to ten times of typical velocity of the bulk flow of water. Thus, in this study, we reduced the sound speed to the value of ten times the typical bulk speed. We define the lowest sound speed amongst the materials as $\tilde{c}_0$ and the "reduction factor" ξ as:

$$\xi = 10 \times \frac{\sqrt{2gH}}{\tilde{c}_0}, \quad \ldots \quad (19)$$

where H is the typical height of the system. Then, the sound speeds listed in **Table 1** are replaced with ξc_0. With this change, we also reduce the shear modulus. Since the shear modulus has the dimension of $\rho_0 c_0^2$, we multiply ξ^2 by the shear modulus values listed in **Table 1**. For our experiment setup, $H \sim 2$ m and $\tilde{c}_0 = 1400$ m/s. Thus, $\xi \sim 0.05$ throughout this study.

This technique allows us to perform numerical simulations much faster because we can take the size of time step much longer than the actual value without losing any fundamental features of flows. Adopting the reduction of sound speed, the sound speeds for all materials in a concerning system become ξ times smaller than the actual value. Recall that the size of time step is determined by the sound speed (see Eqs. (15) and (18)). Note that w_{ij} has a comparable value to $h\nabla\cdot\vec{v}$, thus, in the case of debris flows, w_{ij} is smaller than $c_i + c_j$. Consequently, $v_{ij}^{\rm sig} \sim c_i + c_j$. Adopting the reduction of the sound speed, $v_{ij}^{\rm sig} \to \xi v_{ij}^{\rm sig}$. Hence, the time step determined by CFL condition (left side of the terms in the parenthesis in Eq. (18)) becomes $1/\xi$ times larger.

2.5. Code Parallelization

Particle based numerical simulations require much higher calculation costs than that of mesh simulations, because we need to search neighbor particles amongst all particles for each particle, which means that the calculation costs is $O(N^2)$, where N is the number of particles deployed in a run. In this report, in order to carry out runs quickly, we employed FDPS [10, 11]. FDPS automatically adopts two techniques to perform particle-based numerical simulations quickly. One is the tree method, developed by [23, 24], and another is massively parallelization.

The tree method uses octree structure to search neighbor particles. Firstly, make the "root" cell which contains all particles, and then, divide it to eight same-size sub cells which are called "branch." Then, recursively divide branches into eight sub cells until the branch contains greater than $N_{\rm crit}$ particles. After this procedure finished, then, we can search neighbor particles by traversing tree structure (for detail, see [24]). This method can reduce the calculation costs to $N\log_8 N$. In this report, we set $N_{\rm crit}$ to 16.

Another technique is the massively parallelization using the Message Passing Interface (MPI). To combine massively parallelization and the tree method, FDPS uses "multi-section" method [25] so that each process has roughly the same number of particles.

3. Experimental and Numerical Setups

In order to understand the characteristics of debris flow routing mechanisms and deposition behavior, it is necessary to create an experimental physical model of debris flow. The model comprises three main parts: a rectangular flume, deposition board, and water intake tank. The total length of the rectangular flume is 5 m and the debris is placed 3.5 m from the bottom of the flume. The floor of

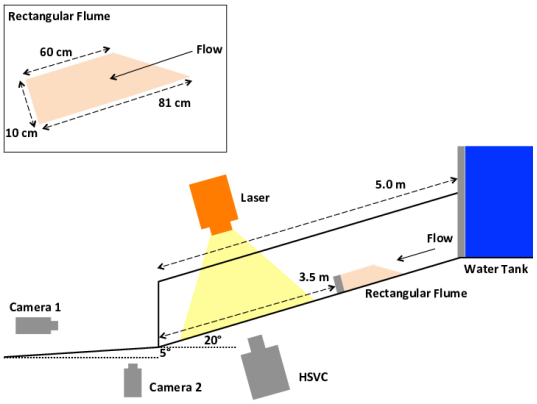

Fig. 1. Illustration of the experimental setups.

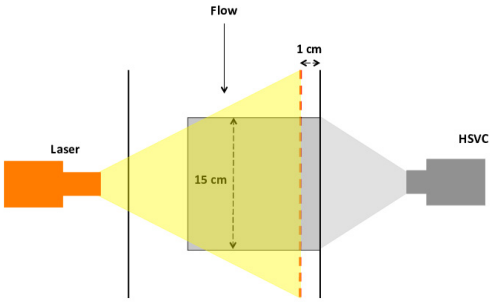

Fig. 2. Test recording on video camera.

the flume is not moving but fixed. The details of the debris loaded in the rectangular flume are shown in **Fig. 1**. The gradient of the rectangular flume is 20°. After the flume and board were set to the prescribed slopes, a constant discharge of water was supplied from the upstream end of the channel through an electromagnetic valve. The constant discharge (3 L/s) was supplied for 7 s.

During the water supply period, the HSVC recorded images of particle routing. The HSVC captured video footage over short time intervals of 0–9 s. It was placed near the downstream of the rectangular flume. To record images of particle routing without effect of roughness from the side of the experimental physical model, a laser beam optical device was used. The laser irradiated the debris flow in a location separated by 1 cm from the side of the experimental physical model, as is shown in **Fig. 2**. Moreover, two video cameras were set at different locations to record the continuous and simultaneous processes of the debris flow deposition.

Firstly, we set the slope by placing the fixed particles. These fixed particles give interactions to the other SPH particles but do not change their positions at all. The density is set to that of aluminum.

Then we placed debris particles composing 20 kg of basaltic rocks. The rocks are in a dry condition. The mass density of the rock is 2.65 g/cm^3. We used one debris size in one experiment: it was 10 mm. In this study, we performed the numerical simulations using a single debris size. The numerical resolutions were then determined so that the radius of one particle became roughly equivalent to that of the actual debris particles. Thus, one debris particle consisted of one SPH particle. Then, we flushed water from the top of the slope at the discharge rate of 3 L/s. The angle of the slope was set to 20°.

4. Results

Before showing the results of numerical simulations which mimicked laboratory experiments, we show the evidence that one debris particle can reproduce necessary features of rock to the experiment. Consider that two debris particles whose diameter are 10 mm collide each other with the relative speed of 6 m/s. We performed numerical simulations of this situation by SPH with two cases; one case is that each debris particles consist of only one particle and another case is the same but consist of 793 particles. Note that in this case, since the typical velocity is 6 m/s and the sound speed of a debris particle is 3116 m/s, we set ξ to $10 \times 6/3116$. Also, to check the applicability of the reduced sound speed technique, we carried out a run with 793 particles but with $\xi = 1$.

Figure 3 shows the results of this test. We can see that in the second row, the positions of two particles are slightly different. In the case of the 793-particles run, two particles are touching each other, whereas in the case of the one-particle run they are off. However, we state that the overall features are the same. The right particle gives its momentum to the left particle and the left particles is popped out.

Figure 4 shows the same to the right column of **Fig. 3** but without the reduction of sound speed. We can see somewhat different velocity distributions to the right column of **Fig. 3**. However, the essential behavior of two debris particles is the same. In the following case, the velocity distributions inside of the debris particles are not important.

Hence, we can conclude that despite one particle, SPH can roughly deal with a collision of two debris particles. Thus, following, we use only one SPH particle to one debris particle.

Here we note that the number of SPH particles which consist of "one" debris particle would eventually change. Recall the right column of **Fig. 3**. In the first and third panel, we can clearly say that two debris particles are separated enough to distinguish them. We, however, state that in the second panel we can see that two debris particles are apparently touching. Consider particles near the contact surface in the debris particle on the right side. Since these particles interact with particles in the debris particle on the left side, they act as if the right debris particle and the left one compose a single continuum, and vice versa. Thus, it is difficult to say the number of SPH particles which composes one continuum.

Here we will provide the comparisons of the numerical results within the early stages of the experiments given in Section 3 and [15]. Several debris particles from our

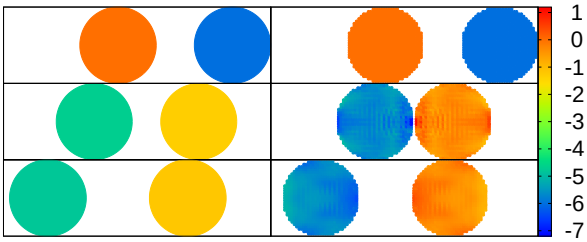

Fig. 3. Snapshots of the collision test. Left column shows the results of one-particle run, whereas the right column shows the same but of 793-particle run. The size of each particle correspond to Hh for each particle. The color bar indicates the x-directional velocity. The snapshot times are $t = 0$, 2.5×10^{-3}, and 5.0×10^{-3} from top to bottom, respectively.

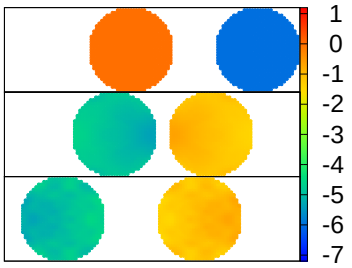

Fig. 4. Same as **Fig. 3**, but without the reduction of sound speed.

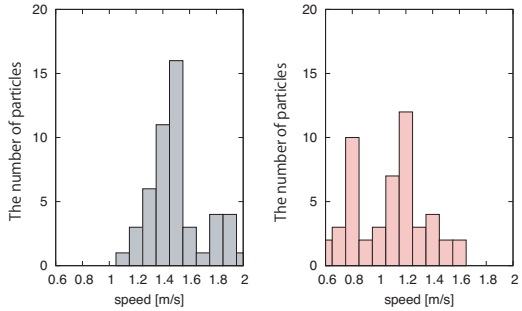

Fig. 5. The binned speed vs. the number of particles is shown. The both panels show that of the "with-flow" frame. The bin width is set to 0.1 m/s. Red rectangles indicate the results of SPH, whereas gray ones indicate those of experiments.

experiments are shown in **Fig. 5**. Hereafter we focus on the behavior of the early stages.

We consider two cases: one is the "no-strength" case, which ignores the shear strength so that only bulk compression works. The second is the "with-strength" case, which considers both the bulk compression and shear strength. Firstly, we show the results of the no-strength case, before considering the with-strength case.

Figures 6 and **7** show snapshots of the "no-flow" and "with-flow" frames respectively for debris of 10 mm in size, which mean the debris particles movement just before and after water flow, each. The qualitative features seem similar to the results of the experiment: the water flow moves debris particles downstream. According to [15], in this frame, several debris particles of 10 mm in size precede the water, while other debris particles float on the water. However, we observed different qualitative features. Whilst [15] showed that the measured velocity of the water is about ~ -2 m/s, SPH predicts a much lower velocity of ~ -1 m/s.

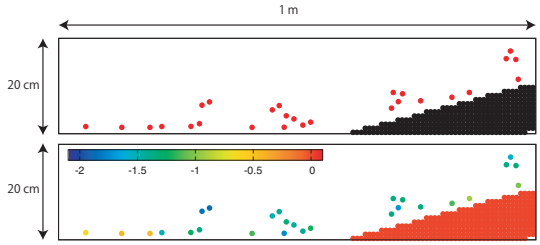

Fig. 6. Snapshots of the "no-flow" frame for the 10-mm debris size. The color of each particle in the upper panel indicates the material. Red, black, and blue particles are debris, slope, and water, respectively. The color of each particle in the lower panel indicates the velocity in the x-direction. The size of each particle is set to the size of SPH particles, viz., Hh. The horizontal length of these panels is 1 m and the vertical length of those is 20 cm.

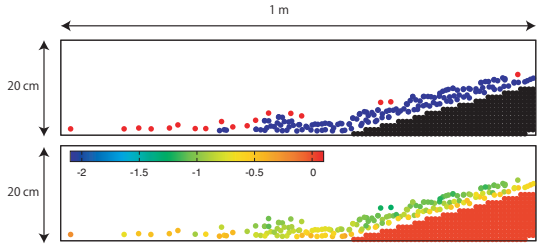

Fig. 7. Equivalent to **Fig. 6**, but showing the "with-flow" frame for the debris size of 10 mm. The horizontal length of these panels is 1 m and the vertical length of those is 20 cm.

Figure 5 shows the quantitative comparison between SPH and experiments. The experimental measurements are obtained similarly to the manner demonstrated in [15]'s. By measuring the distances between each pair of particles, the velocity of each particle can be calculated. Note that we picked 30 particles randomly from all particles in the intermediate stage. We then derived the velocity distributions of the SPH particles around the end of the slope. We can see that the mean speed of SPH particles is lower than that of the experimental particles, especially in the intermediate stage.

We show the results of the "with-strength" model. **Fig. 8** shows the debris particles on the slope. After the water hits the debris particles, it runs over the debris particles before eroding them. However, the amount of the eroded particles is much lower than expected. The eroded particles move to the bottom of the water. However, in this simulation, the debris particles stop in the middle of

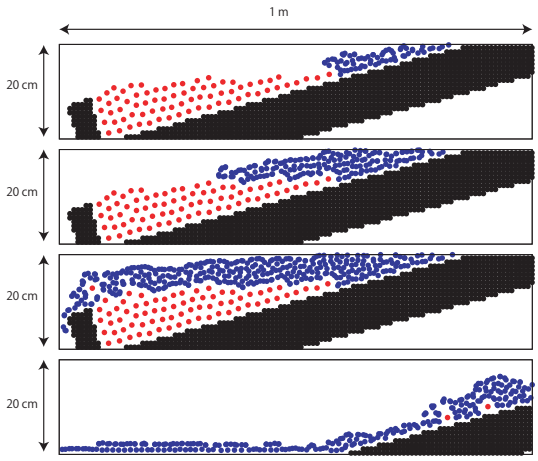

Fig. 8. The top three panels show the time series of the with-strength case around the debris load. In these panels, the horizontal length of these panels is 1 m and the vertical length of those is 20 cm. The last panel shows the deposition area. In this panel, the horizontal length is 1 m and the vertical length is 20 cm. The color of each particle indicates its material.

the slope.

In order to investigate the source of this difference, we review the results of the experiments done in [15]. According to [15], some of the larger debris particles precede the water and while others float on it; smaller debris particles tend to sink. When the water hits the debris particles, they are first pushed and then popped out. These particles can be recorded by HSVC as preceding particles. Meanwhile, the particles carried by the water are from the eroded particles. When the water runs over the debris particles, it drags on and erodes the debris particles. The motions of these eroded particles are controlled by frictional forces.

Combining this discussion with **Fig. 8**, we can conclude that the SPH provided in this study does not have sufficient capability to address drag forces acting among the particles. A much stronger frictional force between particles must exits. Therefore, the debris particles are first eroded by the water, but then decelerate by nonphysical friction. This also causes the sticking behavior of the debris particles deposited in the middle of the slope. One possible reason for the numerical simulations' poor description of the drag force is the poor resolution, particularly for water particles. Macro-scale turbulence generated by mutual interactions between surrounding water and sediments is better illustrated by smaller water particles compared to the mean diameter of the sediments, which has not been established in this numerical simulation. Since debris SPH particles and water SPH particles have equal sizes, a much stronger frictional force may emerge. Otherwise, the poor description of the shear flow by SPH has been reported by several works (e.g., [26–28]). SPH tends to generate large errors in formulating the pressure gradient and/or the AV, which can cause unwanted shear forces.

5. Summary

In this study, we demonstrated the results of numerical simulations of debris flows including the effects of solid mechanics. This was the first attempt to perform a numerical simulation of a debris flow by a fully SPH manner, which could free us from conceptual assumptions for rigid bodies. The validation problem was established as similar to the experiments given in Section 3 and reported in [15]; water was flushed onto debris particles lying in the middle of a slope. The results roughly depicted of two types of debris particles, composing those that preceded the water and those carried by the water. The SPH simulation showed qualitatively similar results, although there are several differences in quantitive comparison. This discrepancy could arise from two factors; one is the resolution and the other is the poor capability of SPH in modeling shear flow. Lately, several novel SPH flavors and formulations to improve the description of shear flow have been suggested (e.g., [26, 29–31]). In addition, FDPS allowed us to deploy a large number of particles easily.

Recent studies about debris flow by SPH [5, 7] solved the interactions between fluid and solid phase by using DEM techniques. They applied the Hertzian contact model to the bulk compression of solid materials and dash-pot models to mimic friction forces between solid materials. Despite the success of this technique, the approach could be limited with applicability only for the less destructive phenomena. Another approach to solve the interactions to between fluid and solid is to solve the equations of elastic bodies. Ma and Geni [9] showed the capability of this approach for modeling the impact of droplets onto solid materials. While this approach is attractive in terms of generality, no existing works has focused on debris flow. However, the results given in this study demonstrate less accurate results for shear-driven debris particles. Since SPH has less dependence on conceptual assumptions, this mismatch is attributed to numerical errors in the SPH formulation, or more simply, to numerical resolution. We will address the problem in a forthcoming study.

Acknowledgements

We thank Mr. Shigeo Fujiki for his help in performing the experiments. The numerical simulations were done on the K computer provided by the RIKEN Advanced Institute for Computational Science. Part of this work was also done on the computer cluster at the Japan Agency for Marine-Earth Science and Technology (JAMSTEC).

References:

[1] S. Egashira, "Prospects of debris flow studies from constitutive relations to governing equations," J. Disaster Res., Vol.6, No.3, pp. 313-320, 2011.

[2] Y. Yamashiki et al., "Simulation and calibration of hydro-debris 2D model (HD2DM) to predict the particle segregation processes in debris flow," J. of Civil Engineering and Architecture, Vol.6, No.6, pp. 690-698, 2012.

[3] R. A. Gingold and J. J. Monaghan, "Smoothed particle hydrodynamics: Theory and application to non-spherical stars," Monthly

Notices of the Royal Astronomical Society, Vol.181, No.3, pp. 375-389, 1977.
[4] L. B. Lucy, "A numerical approach to the testing of the fission hypothesis," The Astronomical J., Vol.82, No.12, pp. 1013-1024, 1977.
[5] R. B. Canelas et al., "Debris flow modelling with high-performance meshless methods," Congress on Numerical Methods in Engineering (CMN2015), 2015.
[6] W. Wang et al., "3D numerical simulation of debris-flow motion using SPH method incorporating non-Newtonian fluid behavior," Natural Hazards, Vol.81, No.3, pp. 1981-1998, 2016.
[7] R. Canelas et al., "A generalized SPH-DEM discretization for the modelling of complex multiphasic free surface flows," 8th Int. SPHERIC Workshop, 2013.
[8] W. Benz and E. Asphaug, "Impact simulations with fracture. I. Method and tests," Icarus, Vol.107, No.1, pp. 98-116, 1994.
[9] X.-J. Ma and M. Geni, "Simulation of droplet impacting on elastic solid with the SPH method," Mathematical Problems in Engineering, Vol.2015, Article No.350496, 2015.
[10] M. Iwasawa et al., "FDPS: A novel framework for developing high-performance particle simulation codes for distributed-memory systems," Proc. of the 5th Int. Workshop on Domain-Specific Languages and High-Level Frameworks for High Performance Computing (WOLFHPC'15), Article No.1, 2015.
[11] M. Iwasawa et al., "Implementation and performance of FDPS: A framework for developing parallel particle simulation codes," Publications of the Astronomical Society of Japan, Vol.68, No.4, Article No.54, 2016.
[12] J. J. Monaghan, "Simulating free surface flows with SPH," J. of Computational Physics, Vol.110, No.2, pp. 399-406, 1994.
[13] B. Zanuttigh and A. Lamberti, "Analysis of debris wave development with one-dimensional shallow-water equations," J. of Hydraulic Engineering, Vol.130, No.4, pp. 293-304, 2004.
[14] S. Hergarten and J. Robl, "Modelling rapid mass movements using the shallow water equations in Cartesian coordinates," Natural Hazards and Earth System Sciences, Vol.15, No.3, pp. 671-685, 2015.
[15] Y. Yamashiki et al., "Experimental study of debris particles movement characteristics at low and high slope," J. of Global Environmental Engineering, Vol.17, pp. 9-18, 2012.
[16] H. J. Melosh, "Impact cratering: A geologic process," Oxford University Press, 1989.
[17] J. J. Monaghan, "Smoothed particle hydrodynamics," Annual Review of Astronomy and Astrophysics, Vol.30, pp. 543-574, 1992.
[18] W. Dehnen and H. Aly, "Improving convergence in smoothed particle hydrodynamics simulations without pairing instability," Monthly Notices of the Royal Astronomical Society, Vol.425, No.2, pp. 1068-1082, 2012.
[19] H. Wendland, "Piecewise polynomial, positive definite and compactly supported radial functions of minimal degree," Advances in Computational Mathematics, Vol.4, No.1, pp. 389-396, 1995.
[20] J. J. Monaghan et al., "Gravity currents descending a ramp in a stratified tank," J. of Fluid Mechatronics, Vol.379, pp. 39-69, 1999.
[21] J. J. Monaghan, "SPH and Riemann solvers," J. of Computational Physics, Vol.136, No.2, pp. 298-307, 1997.
[22] D. S. Balsara, "Von Neumann stability analysis of smoothed particle hydrodynamics – suggestions for optimal algorithms," J. of Computational Physics, Vol.121, No.2, pp. 357-372, 1995.
[23] J. Barnes and P. Hut, "A hierarchical *O (N log N)* force-calculation algorithm," Nature, Vol.324, Issue 6096, pp. 446-449, 1986.
[24] L. Hernquist and N. Katz, "TREESPH: A unification of SPH with the hierarchical tree method," The Astrophysical J. Supplement Series, Vol.70, pp. 419-446, 1989.
[25] J. Makino, "A fast parallel treecode with GRAPE," Publications of the Astronomical Society of Japan, Vol.56, No.3, pp. 521-531, 2004.
[26] N. Hosono, T. R. Saitoh, and J. Makino, "A comparison of SPH artificial viscosities and their impact on the Keplerian disk," The Astrophysical J. Supplement Series, Vol.224, No.2, Article No.32, 2016.
[27] Y. Imaeda and S. Inutsuka, "Shear flows in smoothed particle hydrodynamics," The Astrophysical J., Vol.569, No.1, pp. 501-518, 2002.
[28] T. Okamoto et al., "Momentum transfer across shear flows in smoothed particle hydrodynamic simulations of galaxy formation," Monthly Notices of the Royal Astronomical Society, Vol.345, No.2, pp. 429-446, 2003.
[29] N. Frontiere, C. D. Raskin, and J. M. Owen, "CRKSPH – A conservative reproducing kernel smoothed particle hydrodynamics scheme," J. of Computational Physics, Vol.332, pp. 160-209, 2017.
[30] E. Gaburov and K. Nitadori, "Astrophysical weighted particle magnetohydrodynamics," Monthly Notices of the Royal Astronomical Society, Vol.414, No.1, pp. 129-154, 2011.
[31] D. García-Senz, R. M. Cabezón, and J. A. Escartín, "Improving smoothed particle hydrodynamics with an integral approach to calculating gradients," Astronomy & Astrophysics, Vol.538, Article No.A9, 2012.

Name:
Shoji Ueta

Affiliation:
Research/Teaching Assistant, Center for Planetary Sciences (CPS), Kobe University

Address:
7-1-48 Minatojima-minamimachi, Chuo-ku, Kobe, Hyogo 650-0047, Japan

Brief Career:
2017 Researcher, Kyoto University
2020 Research/Teaching Assistant, Kobe University

Selected Publications:
• S. Ida, S. Ueta, T. Sasaki, and Y. Ishizawa, "Uranian satellite formation by evolution of a water vapour disk generated by a giant impact," Nature Astronomy, Vol.4, No.9, pp. 880-885, 2020.
• S. Ueta and T. Sasaki, "The structure of suaface H_2O layers of ice-covered planets with high-pressure ice," The Astrophysical J., Vol.775, No.2, Article No.96, 2013.

Academic Societies & Scientific Organizations:
• Japanese Society for Planetary Sciences (JSPS)
• Astronomical Society of Japan (ASJ)
• Japan Geoscience Union (JpGU)

Name:
Natsuki Hosono

Affiliation:
Center for Planetary Science (CPS), Kobe University

Address:
7-1-48 Minatojima-minamimachi, Chuo-ku, Kobe, Hyogo 650-0047, Japan

Brief Career:
2014-2016 Postdoctoral Researcher, RIKEN Advanced Institute for Computational Science (AICS)
2016-2017 Assistant Professor, Kyoto University
2017-2020 Postdoctoral Researcher, Japan Agency for Marine-Earth Science and Technology (JAMSTEC)
2020- Assistant Professor, Kobe University

Selected Publications:
• N. Hosono et al., "Terrestrial magma ocean origin of the Moon," Nature Geoscience, Vol.12, No.6, pp. 418-423, 2019.
• N. Hosono et al., "The giant impact simulations with density independent smoothed particle hydrodynamics," Icarus, Vol.271, pp. 131-157, 2016.
• N. Hosono, T. R. Saitoh, and J. Makino, "Density-independent smoothed particle hydrodynamics for a non-ideal equation of state," Publ. Astron. Soc. Jpn., Vol.65, No.5, Article No.108, 2013.

Academic Societies & Scientific Organizations:
• Japanese Society for Planetary Sciences (JSPS)
• Astronomical Society of Japan (ASJ)
• American Geophysical Union (AGU)

Name:
Ryusuke Kuroki

Affiliation:
Mizuho Financial Group, Inc.

Address:
1-1-5 Otemachi, Chiyoda-ku, Tokyo 100-8333, Japan

Brief Career:
2016 B.Sc., Faculty of Science, Kyoto University
2019 M.Phil., Graduate School of Advanced Integrated Studies in Human Survivablity, Kyoto University
2019- Mizuho Financial Group, Inc.

Selected Publications:
• J. Troselj et al., "Modeling of extreme freshwater outflow from the north-eastern Japanese river basins to western Pacific Ocean," J. Hydrol., Vol.555, pp. 956-970, 2017.

Name:
Yosuke Alexandre Yamashiki

Affiliation:
Graduate School of Advanced Integrated Studies in Human Survivability (GSAIS), Kyoto University

Address:
1 Nakaadachi-cho, Yoshida, Sakyo-ku, Kyoto, Kyoto 606-8306, Japan

Brief Career:
1990 B.Eng., Faculty of Engineering, Kyoto University
1994 M.Eng., Escola Politécnica da Universidade de São Paulo
1999 D.Eng., Graduate School of Engineering, Kyoto University
1999-2001 Associate Programme Officer, International Environmental Technology Centre, United Nations Environment Programme (UNEP-IETC)
2001-2004 Assistant Professor, Graduate School of Engineering, Kyoto University
2004-2008 Lecturer, College of Science and Technology, Kyoto University
2008-2013 Associate Professor, Disaster Prevention Research Institute (DPRI), Kyoto University
2014- Professor, GSAIS, Kyoto University

Selected Publications:
• M. Fujita, T. Sato, S. Saito, and Y. Yamashiki, "Probabilistic risk assessment of solar particle events considering the cost of countermeasures to reduce the aviation radiation dose," Scientific Reports, Vol.11, Article No.17091, 2021.
• Y. A. Yamashiki et al., "Impact of stellar superflares on planetary habitability," The Astrophysical J., Vol.881, No.2, Article No.114, 2019.
• Y. Yamashiki et al., "Initial flux of sediment-associated radiocesium to the ocean from the largest river impacted by Fukushima Daiichi Nuclear Power Plant," Scientific Reports, Vol.4, No.3714, 2014.

Academic Societies & Scientific Organizations:
• Oceanographic Society of Japan (JOS)
• Astronomical Society of Japan (ASJ)
• American Geophysical Union (AGU)